

THE POSSIBILITY OF THE SECONDARY OBJECT IN GW190814 AS A NEUTRON STAR

KAIXUAN HUANG¹, JINNIU HU,^{1,2} YING ZHANG^{3,2}, HONG SHEN¹

¹School of Physics, Nankai University, Tianjin 300071, China

²Strangeness Nuclear Physics Laboratory, RIKEN Nishina Center, Wako, 351-0198, Japan

³Department of Physics, Faculty of Science, Tianjin University, Tianjin 300072, China

ABSTRACT

A compact object was observed with a mass $2.50\text{--}2.67 M_{\odot}$ by LIGO Scientific and Virgo collaborations (LVC) in GW190814, which provides a great challenge to the investigations into the supranuclear matter. To study this object, properties of neutron star are systematically calculated within the latest density-dependent relativistic mean-field (DDRMF) parameterizations, which are determined by the ground state properties of spherical nuclei. The maximum masses of neutron star calculated by DD-MEX and DD-LZ1 sets can be around $2.55 M_{\odot}$ with quite stiff equations of state generated by their strong repulsive contributions from vector potentials at high densities. Their maximum speeds of sound c_s/c are smaller than $\sqrt{0.8}$ at the center of neutron star and the dimensionless tidal deformabilities at $1.4 M_{\odot}$ are less than 800. Furthermore, the radii of $1.4 M_{\odot}$ also satisfy the constraint from the observation of mass-radius simultaneous measurements (NICER). Therefore, we conclude that one cannot exclude the possibility of the secondary object in GW190814 as a neutron star composed of hadron matter from DDRMF models.

Keywords: GW190814 - Neutron Star - DDRMF model - Gravitational Waves

1. INTRODUCTION

The rapid progresses of the astronomical observable techniques provide not only great challenges but also many opportunities in the investigations of neutron star. In the past decade, the measurements of massive neutron stars successively broke through our recognition of their maximum masses from PSR J1614-2230 ($1.928 \pm 0.017 M_{\odot}$) (Demorest et al. 2010; Fonseca et al. 2016), PSR J0348+0432 ($2.01 \pm 0.04 M_{\odot}$) (Antoniadis et al. 2013), to PSR J0740+6620 ($2.14^{+0.10}_{-0.09} M_{\odot}$) (Cromartie et al. 2020). For the first time, the mass and radius of PSR J0030+0451 were simultaneously measured by the Neutron star Interior Composition Explorer (NICER) collaboration who drew the first-ever map of neutron star (Raaijmakers et al. 2019). Its was reported to have a mass of $1.44^{+0.15}_{-0.14} M_{\odot}$ with a radius of $13.02^{+1.24}_{-1.06}$ km (Miller et al. 2019) and a mass of $1.34^{+0.15}_{-0.16} M_{\odot}$ with a radius of $12.71^{+1.14}_{-1.19}$ km (Riley et al. 2019) by two independent analysis groups.

At the same time, the multi-messenger astronomy era has begun with the successful operation of gravitational wave detectors, LIGO Scientific and Virgo Collaborations (LVC), which firstly received the gravitational waves generated by a binary neutron-star (BNS) merger GW170817 event (Abbott et al. 2017a,b, 2018). The tidal deformability of neutron star was estimated from the signals, which becomes a new constraint on the equation of state of neutron star matter. The total mass of this BNS system in GW170817 is around $2.7 M_{\odot}$ and the mass of the heavier component is around $1.16 - 1.60 M_{\odot}$ with lower-spin priors, while the maximum mass of neutron star can approach $1.89 M_{\odot}$ with high-spin priors (Abbott et al. 2019). After that, the second possible BNS merger was observed in April of 2019 as GW190425, with the total mass $3.4^{+0.3}_{-0.1} M_{\odot}$. The mass ranges of components are from 1.12 to $2.52 M_{\odot}$ with high-spin priors (Abbott et al. 2020a). Several months later, a new event of a compact binary merger with a $22.2 - 24.3 M_{\odot}$ black hole and a compact component with a mass of $2.50 - 2.67 M_{\odot}$ was reported by LVC as GW190814. The secondary object of GW190814 attracts a lot of attentions, since it may be either the heaviest neutron star or the lightest black hole ever discovered (Abbott et al. 2020b).

Since then, many interesting works were proposed to explain the secondary object of GW190814 in the past several months. Tan et al. considered that it may be a heavy neutron star including the deconfined QCD matter in the

core (Tan et al. 2020). The possibility of a super-fast pulsar was assumed by Zhang et al. (Zhang & Li 2020) and Tsokaros et al. (Tsokaros et al. 2020). Bayesian modeling supported the neutron star with $2.50 - 2.60 M_{\odot}$ under the constraints on the properties of $1.4 M_{\odot}$ neutron star (Lim et al. 2020). On the other hand, it was also concluded that GW190814 may be a binary black hole merger by Fattoyev et al. (Fattoyev et al. 2020) and Tews et al. (Tews et al. 2020).

The mass, radius and tidal deformabilities of neutron star are mainly determined by the equation of state (EOS) of neutron star matter, i. e., the relation between energy density and pressure. Many attempts have been made to obtain the EOS of supranuclear matter in neutron star from different models. It can be assumed as a simple polynomial in terms of pressure and energy density (Annala et al. 2018). It also can be generated by the nuclear density functional theories (DFT) (Vautherin & Brink 1972; Shen et al. 1998; Douchin & Haensel 2001; Shen 2002; Long et al. 2006, 2007; Sun et al. 2008; Dutra et al. 2012; Bao et al. 2014a; Bao & Shen 2014b), where the nucleon-nucleon (NN) interaction was effectively determined by fitting the ground state properties of finite nuclei or the empirical saturation properties of infinite nuclear matter. Moreover, *ab initio* methods with realistic nuclear potentials extracted from NN scattering are available to study the neutron star (Akmal et al. 1998; Li et al. 2006; Carlson et al. 2015; Hu et al. 2017; Sammarruca et al. 2018; Logoteta 2019; Wang et al. 2020).

In these available nuclear many-body models, the EOSs of nuclear matter around the saturation density ($\sim \rho_{B0}$) are well constrained, which corresponds to the central density of finite nuclei (Dutra et al. 2012, 2014). When these EOSs are extrapolated to the supranuclear matter ($\sim 5\rho_{B0}$), most of them can reasonably describe the properties of massive neutron star around $2.0 M_{\odot}$. There are only very few EOSs from the covariant density functional theory (CDFT), which can generate the mass of neutron star above $2.5 M_{\odot}$ such as NL3 parameter set (Lalazissis et al. 1997). However the radius of $1.4 M_{\odot}$ from NL3 is too large to satisfy the recent constraints from the observations of GW170817 and NICER. Therefore, a new parameter set, BigApple, was proposed to generate a $2.6 M_{\odot}$ neutron star and reproduce the observables of finite nuclei and NICER (Fattoyev et al. 2020).

The CDFT has achieved great successes in the fields of nuclear physics and astrophysics. The first available version of CDFT was proposed by Walecka with the Hartree approximation, i. e., the $\sigma - \omega$ model (Walecka 1974), which is also called as relativistic mean-field (RMF) model. Then, the ρ meson, nonlinear terms of σ and ω mesons, and the coupling terms with ρ meson to σ or ω meson were introduced step by step in the RMF model (Serot 1979; Boguta & Bodmer 1977; Sugahara & Toki 1994; Horowitz & Piekarewicz 2001). These nonlinear RMF models can describe the ground state properties of most nuclei in the nuclide chart precisely. Meanwhile, the contributions of the exchange terms in the mean-field approximation were considered at the end of 1970s in the framework of relativistic Hartree-Fock (RHF) model, where the pion effect can be taken into account (Brockmann 1978; Bouyssy et al. 1987; Long et al. 2006, 2007). The picture of meson exchange can be simplified as a point contact interaction when the meson masses are assumed to have an infinite value, which avoids solving the equation of motion for mesons (Nikolaus et al. 1992). This point coupling RMF model is also widely applied to study the nuclear mass table (Zhao et al. 2010). Furthermore, the nonlinear terms of various mesons could be replaced by the density-dependent meson-nucleon coupling constants in the density-dependent RMF (DDRMF) and DDRHF models, which consider the nuclear medium effect originated by the relativistic Brueckner-Hartree-Fock model (Brockmann & Toki 1992).

Ten years ago, it was showed by Sun et al. (Sun et al. 2008) that some parameterizations of DDRMF and DDRHF models generated massive neutron stars around $2.33 - 2.48 M_{\odot}$ such as PKDD (Long et al. 2004), DD-ME1 (Nikić et al. 2002), DD-ME2 (Lalazissis et al. 2005), PKO1, PKO2, and PKO3 (Long et al. 2006) sets, whereas properties of neutron star at $1.4 M_{\odot}$ were not carefully discussed due to the deficiencies of astronomical observables. In 2020, several DDRMF parameters, DD-MEX (Taninah et al. 2020), DD-LZ1 (Wei et al. 2020), and DDV, DDVT, DDVTD (Typel & Terrero 2020) were proposed by different groups by fitting ground state properties of spherical finite nuclei, which considered the parametric correlations, shell evaluations, and tensor couplings of the vector mesons to nucleons, respectively. Therefore, it is necessary to systematically calculate the properties of neutron star with these latest DDRMF parameterizations and discuss the possibility of the secondary object of GW190817 as a neutron star.

This paper is arranged as follows: the theoretical descriptions of DDRMF model and neutron star matter are shown in Sec. 2; in Sec. 3, properties of nuclear matter and neutron star will be presented and discussed with various DDRMF models. The summaries and discussion will be given in Sec. 4.

2. THE DENSITY-DEPENDENT RELATIVISTIC MEAN-FIELD MODEL IN NEUTRON STAR

In DDRMF model, the nucleons usually interact with each other in nuclear system through exchanging the scalar-isoscalar (σ), vector-isoscalar (ω), and vector-isovector (ρ) mesons. In some models, the scalar-isoscalar (δ) meson is also taken into account to consider the isovector effect on the scalar potential of nucleon. The DDRMF Lagrangian

density can be written as:

$$\begin{aligned}
\mathcal{L}_{DD} = & \sum_{i=p, n} \bar{\psi}_i \left[\gamma^\mu \left(i\partial_\mu - \Gamma_\omega(\rho_B)\omega_\mu - \frac{\Gamma_\rho(\rho_B)}{2}\gamma^\mu \vec{\rho}_\mu \vec{\tau} \right) - \left(M - \Gamma_\sigma(\rho_B)\sigma - \Gamma_\delta(\rho_B)\vec{\delta}\vec{\tau} \right) \right] \psi_i \\
& + \frac{1}{2} (\partial^\mu \sigma \partial_\mu \sigma - m_\sigma^2 \sigma^2) + \frac{1}{2} (\partial^\mu \vec{\delta} \partial_\mu \vec{\delta} - m_\delta^2 \vec{\delta}^2) \\
& - \frac{1}{4} W^{\mu\nu} W_{\mu\nu} + \frac{1}{2} m_\omega^2 \omega_\mu \omega^\mu - \frac{1}{4} \vec{R}^{\mu\nu} \vec{R}_{\mu\nu} + \frac{1}{2} m_\rho^2 \vec{\rho}_\mu \vec{\rho}^\mu,
\end{aligned} \tag{1}$$

where, ψ_i represents the wave function of nucleon (proton or neutron). σ , ω_μ , $\vec{\rho}_\mu$, and $\vec{\delta}$ denote the σ , ω , ρ , and δ mesons, respectively. $W_{\mu\nu}$ and $\vec{R}_{\mu\nu}$ are the anti-symmetry tensor fields of ω and ρ mesons. In nuclear matter, the tensor coupling between the vector meson and nucleon does not provide any contributions. Therefore, it is neglected in the present Lagrangian. The coupling constants between mesons and nucleon are density-dependent in DDRMF model, which was firstly proposed by Brockmann and Toki (Brockmann & Toki 1992). It takes into account that the NN interaction in dense matter is affected by nuclear medium. The density-dependent behaviors of the coupling constants have many styles. In CDFT, there are two types of density, i. e., the scalar density (ρ_s) and vector density (ρ_B). In principle, the coupling constants in DDRMF can be dependent on scalar density or vector density. In this work, we focus on the parameterizations of DDRMF depending on the vector density, which only influences the self energy instead of total energy. Coupling constants of σ and ω mesons are usually expressed as a fraction function of the vector density. In DD2 (Nikšić et al. 2002), DD-ME1, DD-ME2, DDME-X, DDV, DDVT, and DDVTD parameterizations, they are given as:

$$\Gamma_i(\rho_B) = \Gamma_i(\rho_{B0})f_i(x), \quad \text{with} \quad f_i(x) = a_i \frac{1 + b_i(x + d_i)^2}{1 + c_i(x + d_i)^2}, \quad x = \rho_B/\rho_{B0}, \tag{2}$$

for $i = \sigma, \omega$. ρ_{B0} is the saturation density of symmetric nuclear matter. Five constraints on the coupling constants $f_i(1) = 1$, $f_i''(0) = 0$, $f_\sigma'(1) = f_\omega'(1)$ can reduce the numbers of independent parameters to three in Eq. (2). The first two constraints lead to

$$a_i = \frac{1 + c_i(1 + d_i)^2}{1 + b_i(1 + d_i)^2}, \quad 3c_i d_i^2 = 1. \tag{3}$$

For the isovector mesons ρ and δ , their coupling constants are,

$$\Gamma_i(\rho_B) = \Gamma_i(\rho_{B0})\exp[-a_i(x - 1)]. \tag{4}$$

While in DD-LZ1 parametrization, the coefficient in front of fraction function, Γ_i is fixed at $\rho_B = 0$ for $i = \sigma, \omega$:

$$\Gamma_i(\rho_B) = \Gamma_i(0)f_i(x), \tag{5}$$

There are only four constraint conditions as $f_i(0) = 1$ and $f_i''(0) = 0$ for σ and ω coupling constants in DD-LZ1. The constraint $f_\sigma''(1) = f_\omega''(1)$ is removed in DD-LZ1 parametrization, which can give more precise shell evaluations of finite nuclei around $Z = 58$ and 92 (Wei et al. 2020). For ρ meson, its coupling constant is also changed accordingly as

$$\Gamma_\rho(\rho_B) = \Gamma_\rho(0)\exp(-a_\rho x). \tag{6}$$

To solve the nuclear many-body system in the DDRMF model, the mean-field approximation must be adopted following the nonlinear RMF models, in which various mesons are treated as classical fields as

$$\sigma \rightarrow \langle \sigma \rangle \equiv \sigma, \quad \omega_\mu \rightarrow \langle \omega_\mu \rangle \equiv \omega, \quad \vec{\rho}_\mu \rightarrow \langle \vec{\rho}_\mu \rangle \equiv \rho, \quad \vec{\delta} \rightarrow \langle \vec{\delta} \rangle \equiv \delta, \quad \langle \psi \rangle \rightarrow \psi. \tag{7}$$

The space components of vector meson are removed in the parity conservation system. In addition, the spatial derivatives about nucleon and mesons are neglected in the infinite nuclear matter due to its transformation invariance.

Finally, using the Euler-Lagrange equation, the equations of motion of nucleon and mesons are obtained:

$$\begin{aligned}
& \sum_{i=p,n} \left[i\gamma^\mu \partial_\mu - \gamma^0 \left(\Gamma_\omega(\rho_B)\omega + \frac{\Gamma_\rho(\rho_B)}{2}\rho\tau_3 + \Sigma_R(\rho_B) \right) - M_i^* \right] \psi_i = 0. \\
& m_\sigma^2 \sigma = \Gamma_\sigma(\rho_B)\rho_s, \\
& m_\omega^2 \omega = \Gamma_\omega(\rho_B)\rho_B, \\
& m_\rho^2 \rho = \frac{\Gamma_\rho(\rho_B)}{2}\rho_3, \\
& m_\delta^2 \delta = \Gamma_\delta(\rho_B)\rho_{s3}.
\end{aligned} \tag{8}$$

The isospin third components of nucleon are defined as $\tau_3 = 1$ and $\tau_3 = -1$ for protons and neutrons, respectively. A rearrangement term Σ_R will be introduced into Eq. (8) due to the density dependence of coupling constants,

$$\Sigma_R(\rho_B) = -\frac{\partial \Gamma_\sigma(\rho_B)}{\partial \rho_B} \sigma \rho_s - \frac{\partial \Gamma_\delta(\rho_B)}{\partial \rho_B} \delta \rho_{s3} + \frac{\partial \Gamma_\omega(\rho_B)}{\partial \rho_B} \omega \rho_B + \frac{1}{2} \frac{\partial \Gamma_\rho(\rho_B)}{\partial \rho_B} \rho \rho_3, \tag{9}$$

where the scalar, vector densities, and their isospin components are generated by the expectation value of nucleon fields,

$$\begin{aligned}
\rho_s &= \langle \bar{\psi} \psi \rangle = \rho_{sp} + \rho_{sn}, & \rho_{s3} &= \langle \bar{\psi} \tau_3 \psi \rangle = \rho_{sp} - \rho_{sn}, \\
\rho_B &= \langle \psi^\dagger \psi \rangle = \rho_{Bp} + \rho_{Bn}, & \rho_3 &= \langle \psi^\dagger \tau_3 \psi \rangle = \rho_{Bp} - \rho_{Bn}.
\end{aligned} \tag{10}$$

The effective masses of nucleons in Eq. (8) are dependent on the scalar mesons σ and δ ,

$$\begin{aligned}
M_p^* &= M - \Gamma_\sigma(\rho_B)\sigma - \Gamma_\delta(\rho_B)\delta, \\
M_n^* &= M - \Gamma_\sigma(\rho_B)\sigma + \Gamma_\delta(\rho_B)\delta
\end{aligned} \tag{11}$$

and the corresponding effective energies of nucleons have the following form because of the mass-energy relation,

$$E_{Fi}^* = \sqrt{k_{Fi}^2 + (M_i^*)^2}, \tag{12}$$

where k_{Fi} is the Fermi momentum of nucleon.

With the energy-momentum tensor in a uniform system, the energy density, \mathcal{E} and pressure, P of infinite nuclear matter can be obtained respectively as

$$\begin{aligned}
\mathcal{E}_{DD} &= \frac{1}{2} m_\sigma^2 \sigma^2 - \frac{1}{2} m_\omega^2 \omega^2 - \frac{1}{2} m_\rho^2 \rho^2 + \frac{1}{2} m_\delta^2 \delta^2 + \Gamma_\omega(\rho_B)\omega\rho_B + \frac{\Gamma_\rho(\rho_B)}{2}\rho\rho_3 + \mathcal{E}_{\text{kin}}^p + \mathcal{E}_{\text{kin}}^n, \\
P_{DD} &= \rho_B \Sigma_R(\rho_B) - \frac{1}{2} m_\sigma^2 \sigma^2 + \frac{1}{2} m_\omega^2 \omega^2 + \frac{1}{2} m_\rho^2 \rho^2 - \frac{1}{2} m_\delta^2 \delta^2 + P_{\text{kin}}^p + P_{\text{kin}}^n,
\end{aligned} \tag{13}$$

where, the contributions from kinetic energy are

$$\begin{aligned}
\mathcal{E}_{\text{kin}}^i &= \frac{\gamma}{2\pi^2} \int_0^{k_{Fi}} k^2 \sqrt{k^2 + M_i^{*2}} dk = \frac{\gamma}{16\pi^2} \left[k_{Fi} E_{Fi}^* \left(2k_{Fi}^2 + M_i^{*2} \right) + M_i^{*4} \ln \frac{M_i^*}{k_{Fi} + E_{Fi}^*} \right], \\
P_{\text{kin}}^i &= \frac{\gamma}{6\pi^2} \int_0^{k_{Fi}} \frac{k^4 dk}{\sqrt{k^2 + M_i^{*2}}} = \frac{\gamma}{48\pi^2} \left[k_{Fi} \left(2k_{Fi}^2 - 3M_i^{*2} \right) E_{Fi}^* + 3M_i^{*4} \ln \frac{k_{Fi} + E_{Fi}^*}{M_i^*} \right].
\end{aligned} \tag{14}$$

$\gamma = 2$ is the spin degeneracy factor. The binding energy per nucleon can be defined by

$$\frac{E}{A} = \frac{\mathcal{E}}{\rho_B} - M. \tag{15}$$

The symmetry energy is calculated by

$$E_{\text{symDD}} = \frac{1}{2} \frac{\partial^2 E/A}{\partial \beta^2}, \tag{16}$$

where β is the asymmetry factor, defined as $\beta = (\rho_{Bn} - \rho_{Bp})/(\rho_{Bn} + \rho_{Bp})$ and its slope, L_{DD} is given by

$$L_{DD} = 3\rho_B \left. \frac{\partial E_{\text{symDD}}}{\partial \rho_B} \right|_{\rho_B = \rho_{B0}}. \tag{17}$$

Actually, both of them can be derived analytically in RMF model (Dutra et al. 2014).

The scalar potential and vector potential of nucleon are expressed as,

$$U_S = \Gamma_\sigma(\rho_B)\sigma + \Gamma_\delta(\rho_B)\delta\tau_3, \quad (18)$$

$$U_V = \Gamma_\omega(\rho_B)\omega + \frac{1}{2}\Gamma_\rho(\rho_B)\rho\tau_3 + \left[-\frac{\partial\Gamma_\sigma(\rho_B)}{\partial\rho_B}\sigma\rho_s - \frac{\partial\Gamma_\delta(\rho_B)}{\partial\rho_B}\delta\rho_{s3} + \frac{\partial\Gamma_\omega(\rho_B)}{\partial\rho_B}\omega\rho_B + \frac{1}{2}\frac{\partial\Gamma_\rho(\rho_B)}{\partial\rho_B}\rho\rho_3 \right], \quad (19)$$

where the derivative terms in the vector potential originate from the density dependence of coupling constants.

The outer core part of a neutron star, which almost dominates its mass and radius, is usually treated as the uniform matter composed of neutron, proton, and leptons. They are stably existing with the conditions of beta equilibrium and charge neutrality. Therefore the chemical potentials of nucleons and leptons are very important, that can be derived from the thermodynamics equations at zero temperature,

$$\mu_{Bi} = \sqrt{k_{Fi}^2 + M_i^{*2}} + \left[\Gamma_\omega(\rho_B)\omega + \frac{\Gamma_\rho(\rho_B)}{2}\rho\tau_3 + \Sigma_R(\rho_B) \right], \quad (20)$$

$$\mu_l = \sqrt{k_{Fl}^2 + m_l^2}.$$

In neutron star matter, with the density increasing, the muon will be onset when the electron chemical potential μ_e is larger than the muon rest mass, i. e., $\mu_e > m_\mu = 106.55$ MeV. Hence, the beta equilibrium condition now can be expressed by

$$\mu_\mu = \mu_e = \mu_n - \mu_p. \quad (21)$$

The charge neutrality condition has the following form:

$$\rho_{Bp} = \rho_e + \rho_\mu. \quad (22)$$

The pressure and energy density will be obtained as a function of nucleon density within the constraints of Eqs. (21) and (22). The Tolman-Oppenheimer-Volkoff (TOV) equation (Tolman 1939; Oppenheimer & Volkoff 1939) describes a spherically symmetric star in the gravitational equilibrium from general relativity,

$$\frac{dP}{dr} = -\frac{GM(r)\mathcal{E}(r)}{r^2} \frac{\left[1 + \frac{P(r)}{\mathcal{E}(r)}\right] \left[1 + \frac{4\pi r^3 P(r)}{M(r)}\right]}{1 - \frac{2GM(r)}{r}}, \quad (23)$$

$$\frac{dM(r)}{dr} = 4\pi r^2 \mathcal{E}(r),$$

where P and M are the pressure and mass of neutron star at r . Furthermore, the tidal deformability becomes a typical property of neutron star after the observation of the gravitational wave from BNS merger, which characterizes the deformation of a compact object in an external field generated by another star. The tidal deformability of a neutron star can be reduced as dimensionless form,

$$\Lambda = \frac{2}{3}k_2 C^{-5}. \quad (24)$$

where $C = GM/R$ is the compactness parameter. The second order Love number k_2 (Hinderer 2008; Hinderer et al. 2010) is given by

$$k_2 = \frac{8C^5}{5}(1 - 2C)^2 [2 + 2C(\mathcal{Y}_R - 1) - \mathcal{Y}_R] \left\{ 2C [6 - 3\mathcal{Y}_R + 3C(5\mathcal{Y}_R - 8)] \right. \\ \left. + 4C^3 [13 - 11\mathcal{Y}_R + C(3\mathcal{Y}_R - 2) + 2C^2(1 + \mathcal{Y}_R)] \right. \\ \left. + 3(1 - 2C)^2 [2 - \mathcal{Y}_R + 2C(\mathcal{Y}_R - 1)\ln(1 - 2C)] \right\}^{-1}. \quad (25)$$

Here, $\mathcal{Y}_R = y(R)$. $y(r)$ satisfies the following first-order differential equation,

$$r \frac{dy(r)}{dr} + y^2(r) + y(r)F(r) + r^2 Q(r) = 0, \quad (26)$$

where $F(r)$ and $Q(r)$ are functions related to the pressure and energy density

$$F(r) = \left[1 - \frac{2M(r)}{r}\right]^{-1} \{1 - 4\pi r^2[\mathcal{E}(r) - P(r)]\}, \quad (27)$$

$$r^2 Q(r) = \left\{4\pi r^2 \left[5\mathcal{E}(r) + 9P(r) + \frac{\mathcal{E}(r) + P(r)}{\frac{\partial P}{\partial \mathcal{E}}(r)}\right] - 6\right\} \times \left[1 - \frac{2M(r)}{r}\right]^{-1}$$

$$- \left[\frac{2M(r)}{r} + 2 \times 4\pi r^2 P(r)\right]^2 \times \left[1 - \frac{2M(r)}{r}\right]^{-2}.$$

The second Love number corresponds to the initial condition $y(0) = 2$. It is also related to the speed of sound in compact matter, c_s

$$c_s^2 = \frac{\partial P(\varepsilon)}{\partial \mathcal{E}}. \quad (28)$$

3. THE RESULTS AND DISCUSSIONS

Firstly, masses of nucleons and mesons, coupling constants between nucleon and mesons, and saturation densities of symmetric nuclear matter, ρ_{B0} in DD2 (Typel et al 2010), DD-ME1 (Nikšić et al. 2002), DD-ME2 (Lalazissis et al. 2005), DDME-X (Taninah et al. 2020), DDV, DDVT, DDVTD (Typel & Terrero 2020), and DD-LZ1 (Wei et al. 2020) sets are all listed in Table 1,

Table 1. Masses of nucleons and mesons, meson coupling constants, and the nuclear saturation densities in various DDRMF models.

	DD-LZ1		DD2	DD-ME1	DD-ME2	DD-MEX	DDV	DDVT	DDVTD
m_n [MeV]	938.900000	m_n	939.56536	939.0000	939.0000	939.0000	939.565413	939.565413	939.565413
m_p [MeV]	938.900000	m_p	938.27203	939.0000	939.0000	939.0000	938.272081	938.272081	938.272081
m_σ [MeV]	538.619216	m_σ	546.212459	549.5255	550.1238	547.3327	537.600098	502.598602	502.619843
m_ω [MeV]	783.0000	m_ω	783.0000	783.0000	783.0000	783.0000	783.0000	783.0000	783.0000
m_ρ [MeV]	769.0000	m_ρ	763.0000	763.0000	763.0000	763.0000	763.0000	763.0000	763.0000
m_δ [MeV]	—	m_δ	—	—	—	—	—	—	980.0000
$\Gamma_\sigma(0)$	12.001429	$\Gamma_\sigma(\rho_{B0})$	10.686681	10.4434	10.5396	10.7067	10.136960	8.382863	8.379269
$\Gamma_\omega(0)$	14.292525	$\Gamma_\omega(\rho_{B0})$	13.342362	12.8939	13.0189	13.3388	12.770450	10.987106	10.980433
$\Gamma_\rho(0)$	15.150934	$\Gamma_\rho(\rho_{B0})$	7.25388	7.6106	7.3672	7.2380	7.84833	7.697112	8.06038
$\Gamma_\delta(0)$	—	$\Gamma_\delta(\rho_{B0})$	—	—	—	—	—	—	0.8487420
ρ_{B0} [fm ⁻³]	0.158100	ρ_{B0}	0.149	0.152	0.152	0.153	0.1511	0.1536	0.1536
a_σ	1.062748	a_σ	1.357630	1.3854	1.3881	1.3970	1.20993	1.20397	1.19643
b_σ	1.763627	b_σ	0.634442	0.9781	1.0943	1.3350	0.21286844	0.19210314	0.19171263
c_σ	2.308928	c_σ	1.005358	1.5342	1.7057	2.0671	0.30798197	0.27773566	0.27376859
d_σ	0.379957	d_σ	0.575810	0.4661	0.4421	0.4016	1.04034342	1.09552817	1.10343705
a_ω	1.059181	a_ω	1.369718	1.3879	1.3892	1.3936	1.23746	1.16084	1.16693
b_ω	0.418273	b_ω	0.496475	0.8525	0.9240	1.0191	0.03911422	0.04459850	0.02640016
c_ω	0.538663	c_ω	0.817753	1.3566	1.4620	1.6060	0.07239939	0.06721759	0.04233010
d_ω	0.786649	d_ω	0.638452	0.4957	0.4775	0.4556	2.14571442	2.22688558	2.80617483
a_ρ	0.776095	a_ρ	0.518903	0.5008	0.5647	0.6202	0.35265899	0.54870200	0.55795902
a_δ	—	a_δ	—	—	—	—	—	—	0.55795902

The mass of σ meson is fitted as a free parameter in DDRMF model. The coefficients of meson coupling constants, Γ_i in DD-LZ1 are the values at zero density, while other parameter sets adopted the values at nuclear saturation densities. The magnitudes of $\Gamma_\sigma(\rho_{B0})$, $\Gamma_\omega(\rho_{B0})$ and $\Gamma_\rho(\rho_{B0})$ in DD2, DDME-1, DD-ME2, DD-MEX, DDV are consistent with each other. The tensor couplings between vector mesons and nucleon were considered in DDVT and DDVTD, where $\Gamma_\sigma(\rho_{B0})$ and $\Gamma_\omega(\rho_{B0})$ have significant differences comparing to other parameter sets. In addition, the δ meson is included in DDVTD set.

To show the density-dependent behaviors of these coupling constants more clearly, they are plotted as functions of the vector density in Fig. 1. It can be found that all of these coupling constants decrease when the nuclear density becomes larger due to the nuclear medium effect. For the ρ meson coupling constants in panel (c), all parameter sets have very similar density-dependent behaviors in the whole density region. In DDVT and DDVTD, the tensor coupling constants play obvious roles in finite nuclei due to their derivative forms, however, they do not provide any contribution

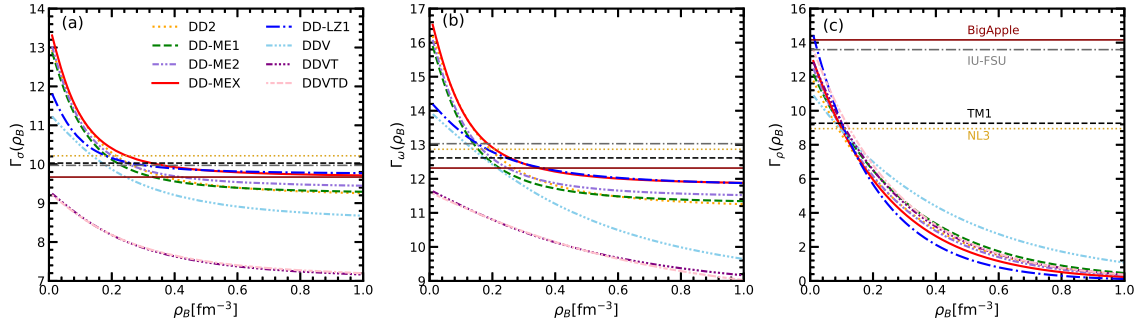


Figure 1. The coupling constants of ω , σ , and ρ mesons as functions of vector density in various DDRMF models and several nonlinear RMF models.

in nuclear matter. Their coupling constants of σ and ω mesons in panel (a) and panel (b) are dramatically smaller than other sets. Furthermore, the coupling constants from several typical nonlinear RMF models, NL3 (Lalazissis et al. 1997), TM1 (Sugahara & Toki 1994), IUFSU (Horowitz & Piekarewicz 2001), and BigApple (Fattoyev et al. 2020) are also shown to compare their differences with those in DDRMF model. At low density region, the coupling constants in DDRMF models are usually stronger than those in nonlinear RMF modes, while weaker at higher density.

With these DDRMF parameter sets, the saturation properties of nuclear matter can be calculated, such as the saturation density, binding energy, incompressibility, symmetry energy, the slope of symmetry energy, and the effective nucleon mass. In Table 2, these properties calculated by various DDRMF models are listed, whose uncertainties of different parameter sets are very small in saturation density, binding energy, incompressibility, and symmetry energy. The slopes of symmetry energy from different models, L are around 40 – 70 MeV, which also satisfy the recent constraints, $L = 59.57 \pm 10.06$ MeV (Zhang et al. 2020). On the other hand, the effective nucleon masses in DDVT and DDVTD are relatively larger, since their scalar coupling strengths are much smaller comparing to other sets.

Table 2. Nuclear matter properties at saturation density generated by present DDRMF parameterizations.

	DD-LZ1	DD2	DD-ME1	DD-ME2	DD-MEX	DDV	DDVT	DDVTD
$\rho_{B0}[\text{fm}^{-3}]$	0.1585	0.149	0.152	0.152	0.1518	0.1511	0.1536	0.1536
$E/A[\text{MeV}]$	-16.126	-16.916	-16.668	-16.233	-16.14	-16.097	-16.924	-16.915
$K_0[\text{MeV}]$	231.237	241.990	243.881	251.306	267.059	239.499	239.999	239.914
$E_{\text{sym}}[\text{MeV}]$	32.016	31.635	33.060	32.31	32.269	33.589	31.558	31.817
$L[\text{MeV}]$	42.467	54.933	55.428	51.265	49.692	69.646	42.348	42.583
M_n^*/M	0.558	0.563	0.578	0.572	0.556	0.586	0.667	0.667
M_p^*/M	0.558	0.562	0.578	0.572	0.556	0.585	0.666	0.666

The binding energies per nucleon for symmetric nuclear matter in panel (a) of Fig. 2 and pure neutron matter in panel (b) of Fig. 2 as functions of vector density are plotted with the present DDRMF parameterizations. These equations of state (EOSs) of nuclear matter below 0.2 fm^{-3} are almost identical since all the parameters were determined by properties of finite nuclei, whose central density is around nuclear saturation density $\rho_{B0} \sim 0.15 \text{ fm}^{-3}$. Their differences increase from 0.30 fm^{-3} . In symmetric nuclear matter, they are separated into the softer group with DDV, DDVT, and DDVTD, and the stiffer group with DD2, DD-ME1, DD-ME2, DD-MEX, and DD-LZ1. The scalar and vector coupling strengths in softer group sets are obviously weaker than those in stiffer group sets. The binding energy of pure neutron matter from DDV is larger than the ones from DDVT and DDVTD. The DDV set has the largest slope of symmetry energy in the present DDRMF parameterizations. This slope will determine the density dependent behaviors of symmetry energy and the binding energy of pure neutron matter, due to $E/A(\beta = 1) \approx E/A(\beta = 0) + E_{\text{sym}}$ at a fixed density.

In general, it is very difficult to measure properties of nuclear matter above twice nuclear saturation density from finite nuclei. Recently, the experiments about heavy-ion collisions provide us some useful information to constrain the EOS of nuclear matter at high density. In Fig. 3, the pressures in symmetric nuclear matter as functions of density from various DDRMF models are shown and compared to the constraints from heavy-ion collisions at $2-4\rho_{B0}$ by Danielewicz et al. (Danielewicz et al. 2002). We can find that the EOSs from the softer group sets are completely consistent with

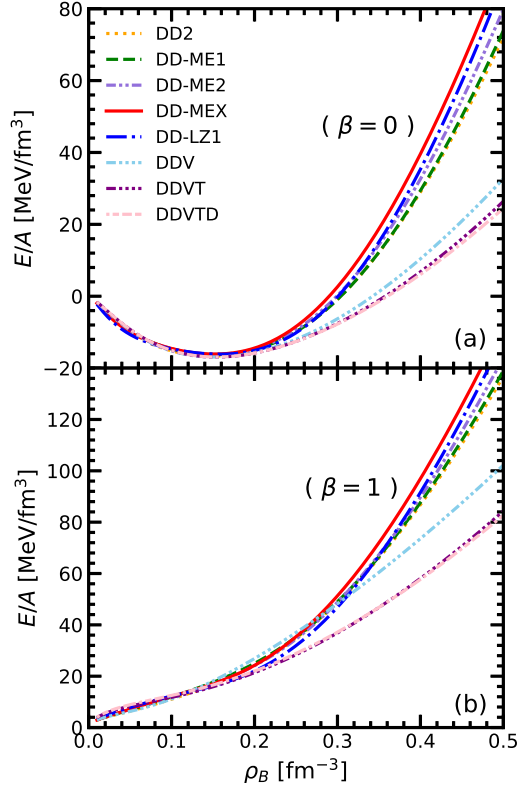


Figure 2. Equations of state of symmetric nuclear matter($\beta = 0$) in panel (a) and pure neutron matter($\beta = 1$) in panel(b) from various DDRMF models.

the experiment data, while the other group is indeed stiffer than the heavy-ion collisions constraints. We also notice that the BigApple and NL3 sets also have the similar situations in the work by Fattoyev et al. (Fattoyev et al. 2020). However, we want to emphasize here that the constraints from the heavy-ion collisions are strongly model-dependent, which is determined by many inputs, such as the NN interaction. To our knowledge, there were few investigations about heavy-ion collisions, which adopted the RMF model as NN interaction. Therefore, it cannot certainly claim that the EOSs generated by DD2, DD-ME1, DD-ME2, DD-MEX, and DD-LZ1 parameterizations are clearly excluded by the constraints of heavy-ion collisions.

To explain the stiff EOSs at high density of DD2, DD-ME1, DD-ME2, DD-MEX, and DD-LZ1 sets, the vector potentials in panel (a) of Fig. 4 and scalar potentials in panel (b) of Fig. 4 for symmetric nuclear matter from present DDRMF parameterizations are shown. The scalar potentials in these sets are very similar, while the vector potentials from different parameter sets have significant differences. The softer group sets provide the weakest vector potentials, which have the analogous magnitudes to the scalar potentials of nucleon. On the other hand, the DD-ME2, DD-MEX, and DD-LZ1 generate the strongest vector components, which are almost twice of those from DDV, DDVT, and DDVTD, because their ω coupling constants are largest at high density regions. Therefore, they provide very stiff EOSs.

Together with the conditions of beta equilibrium and charge neutrality, the EOSs of neutron star matter with DDRMF model can be obtained in Fig. 5, which shows the pressures of neutron star matter as a function of energy density. At crust part of neutron star, the EOS in the non-uniform matter generated by TM1 parameterization with Thomas-Fermi approximation is adopted. In the core of neutron star, EOSs of the uniform matter are calculated with various DDRMF sets. Their density-dependent behaviors are very similar with those in symmetric nuclear matter. At high density region, the stiffer group sets provide higher pressures due to the stronger vector potentials. The joint constraints on EOS extracted from the GW170817 and GW190814 are shown as a shaded band here. When the energy density is smaller than $600 \text{ MeV}/\text{fm}^3$, the EOSs from stiffer group sets satisfy the constraints from the gravitational

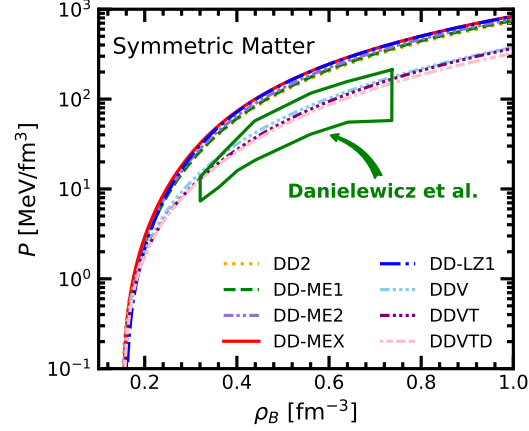


Figure 3. Pressures as a function of vector density of symmetric nuclear matter with various DDRMF parameter sets and the constraints from the heavy ion collisions.

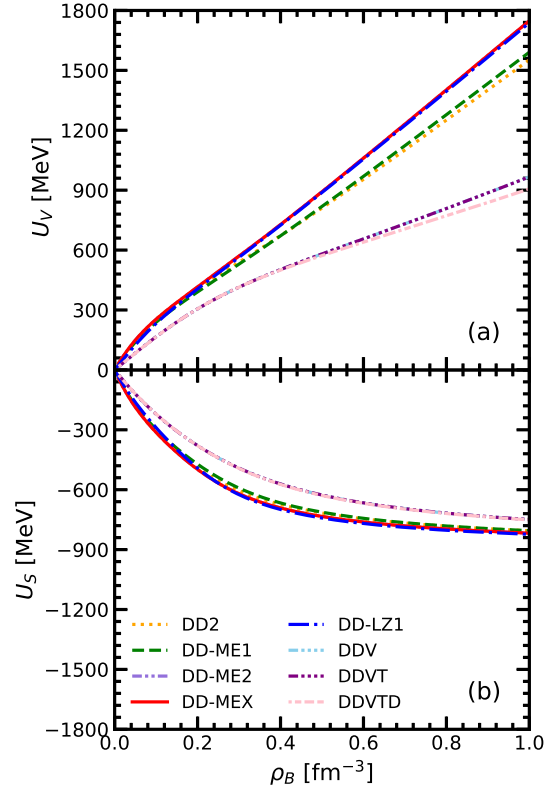


Figure 4. Scalar and vector potentials as a function of the vector density from various DDRMF models.

wave detection. While, the pressures obtained from softer group sets start to be lower than the constraint band from $\varepsilon = 300 \text{ MeV}/\text{fm}^3$. Furthermore, the EOS from TM1 set is also given, which is stiffer than those from DDRMF at intermediate density region and becomes softer when density is creasing. Since, the slope of symmetry energy in TM1 is around 110 MeV. It is much larger than those derived from present DDRMF models, whose L are around 40 – 70 MeV. The slope of symmetry energy mainly influences the pressures in intermediate density. At higher density, the vector potentials in DDRMF from the stiffer group sets are stronger than the one in TM1.

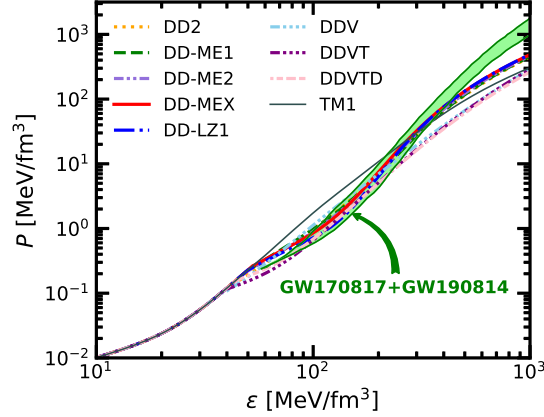


Figure 5. The pressure P versus energy density ε of neutron star matter from DDRMF models and joint constraints from GW170817 and GW190814.

In Fig. 6, the pressures as functions of density in neutron star matter from DDRMF models are given. The pressures from the stiffer group sets are obviously larger than those generated by the softer group sets. The speeds of sound in neutron star matter, c_s with the unit of light speed are plotted in the insert. The c_s^2 from softer group sets are much lower than those from other parameterizations, which are around 0.6 at $\rho_B = 1.0 \text{ fm}^{-3}$. They are consistent with the results from nonlinear RMF models (Hu et al. 2020). The speed of sound from stiffer group EOSs rapidly increase from $\rho_B = 0.2 \text{ fm}^{-3}$ and c_s^2 reach around 0.8 at high density. They will be constants less than one as the density continues growing. Actually, the EOS and speed of light of BigApple set in nonlinear RMF model are very similar with the present work, where a $\omega - \rho$ coupling term was included to reduce the slope of symmetry energy and its vector-isovector coupling constant is very strong as we shown in Fig. 1 (Fattoyev et al. 2020).

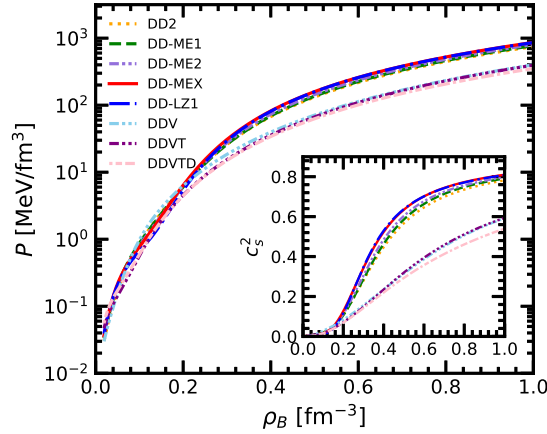


Figure 6. EOSs of neutron star matter with different DDRMF models. The corresponding speeds of sound in units of the speed of light shown in insert.

The mass-radius relation of a static neutron star can be solved by TOV equation Eq. (23), where the EOS of neutron star matter is used. In Fig 7, the mass-radius ($M - R$) relation in panel (a) and mass-central density ($M - \rho_B$) relation in panel (b) from various DDRMF models are shown. From the panel (a), it can be found that the maximum masses of neutron star in softer group sets are around $1.85 - 1.93 M_\odot$ and the corresponding radii are $9.85 - 10.34 \text{ km}$. These results only can explain the existence of PSR J1614-2230 ($1.928 \pm 0.017 M_\odot$). As we discussed before, the EOSs from these three parameter sets are relatively soft due to their small vector potentials. The maximum masses calculated by DD2, DD-ME1, and DD-ME1 sets are about $2.42 - 2.48 M_\odot$, which are consistent with the available investigations (Sun et al. 2008). DD-MEX and DD-LZ1 can support the neutron star above $2.5 M_\odot$ because of their strongest repulsive contributions from ω meson. Their maximum masses can approach $2.56 M_\odot$, which are in accord with the observed mass of the secondary compact object in GW190814, $2.50 - 2.67 M_\odot$. In addition to the constraints

from the observables of massive neutron stars, PSR J1614-2230, PSR J034+0432, and PSR J0740+6620, recently the mass and radius of neutron star at intermediate mass region were measured simultaneously for PSR J0030+0451 by NICER. Its mass and radius were reported around $1.4 M_{\odot}$ and 13 km (Miller et al. 2019; Riley et al. 2019). These constraints from NICER are plotted in panel (a). It can be found that the $M - R$ relations from stiffer group parameterizations around $1.4 M_{\odot}$ completely satisfy the observables from NICER, while the radii of neutron star at $1.4 M_{\odot}$, $R_{1.4}$ from DDVT, and DDVTD are around 11.4 km, which are smaller than the possible radii of J0030+0451. The $R_{1.4}$ of DDV is 12.2 km since its slope of symmetry energy is obviously larger than those of DDVT and DDVTD. When the isoscalar properties of RMF models are the same, the slope of symmetry energy can influence the radii of neutron star at $1.4 M_{\odot}$ in our recent investigations (Ji et al. 2019; Hu et al. 2020).

The $M - \rho_B$ relations in panel (b) from present DDRMF models can be separated by two groups. The first group only can generate the neutron star around $1.9 M_{\odot}$ at the central densities $\sim 8\rho_{B0}$ from softer group EOSs. The second group can support neutron stars around $2.5 M_{\odot}$, where the central densities locate at $5\rho_{B0}$. The corresponding speeds of sound are less than $\sqrt{0.8}c$ from Fig. 6.

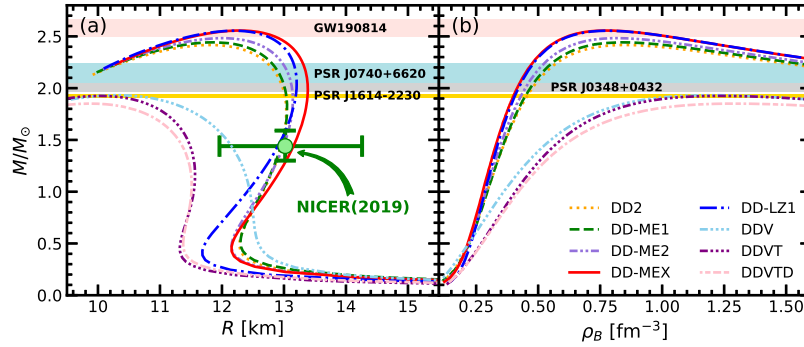


Figure 7. The neutron star masses as functions of radius and the central baryon density. Constraints from astronomical observables for massive neutron star and NICER are also shown.

With the rapid developments of gravitational wave detectors, the tidal deformability of neutron star can be extracted from the BNS merger. It can be calculated with the Love number by solving a first-order differential equation, Eq. (25). In Fig. 8, the dimensionless tidal deformabilities, Λ , of neutron star as function of their masses from DDRMF models are shown. These dimensionless tidal deformabilities decrease with the neutron star mass and become very small at the maximum masses. Their values in softer group sets are significantly lower than those from other parameterizations, since $\Lambda \propto R^5$ approximately from Eq. (24). The radii of neutron star from the softer group EOSs are smaller comparing to the stiffer EOSs. The corresponding Λ at $1.4 M_{\odot}$, $\Lambda_{1.4}$ are from 274.91 to 390.01, while recent analysis by LVC gives $\Lambda_{1.4} = 190^{+390}_{-120}$ from GW170817 (Abbott et al. 2018). Due to the larger radii and speeds of sound of neutron star in stiffer group EOSs, their Λ are relatively higher and $\Lambda_{1.4}$ are between 639.03 and 790.01. Furthermore, the tidal deformabilities at $2.0 M_{\odot}$ from these two types of EOSs have obviously differences. For the softer EOSs, Λ almost approach to zero, while they are around 100 for the stiffer EOSs at $2.0 M_{\odot}$. Once the BNS merger, whose components are around $2 M_{\odot}$, is more precisely measured by the advanced gravitational wave detectors in the future, the EOSs of neutron star can hopefully be determined well. Due to the large uncertainties in the present estimations of tidal deformability, we think that it cannot exclude the possibilities of stiffer EOSs with larger speeds of sound in neutron star, such as those from the stiffer group parameterizations. Therefore, the secondary compact object in GW190814 may be a neutron star.

Finally, properties of neutron star, i. e., the maximum mass (M_{\max}/M_{\odot}), the corresponding radius (R_{\max}), the central density density(ρ_c), the radius ($R_{1.4}$) and dimensionless tidal deformability ($\Lambda_{1.4}$) at $1.4 M_{\odot}$ from present DDRMF models are listed in Table 3, respectively.

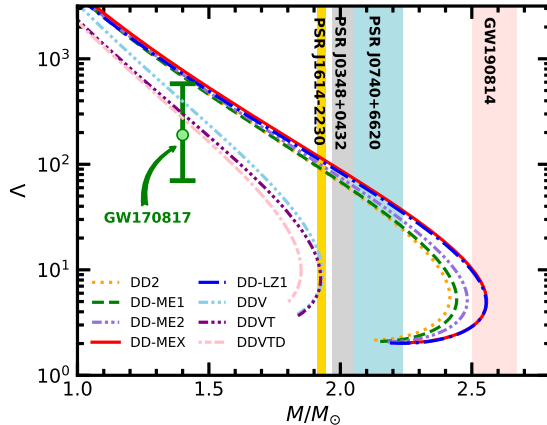


Figure 8. The tidal deformabilities from various DDRMF models as functions of neutron star mass. The mass regions of massive neutron stars are also plotted.

Table 3. Neutron star properties from various DDRMF models.

	DD-LZ1	DD2	DD-ME1	DD-ME2	DD-MEX	DDV	DDVT	DDVTD
M_{\max}/M_{\odot}	2.5545	2.4168	2.4426	2.4829	2.5566	1.9317	1.9251	1.8507
$R_{\max}[\text{km}]$	12.178	11.826	11.885	12.012	12.274	10.336	10.023	9.850
$\rho_{\max}[\text{fm}^{-3}]$	0.786	0.845	0.832	0.813	0.777	1.188	1.237	1.306
$R_{1.4}[\text{km}]$	12.864	12.938	12.931	12.961	13.118	12.195	11.511	11.396
$\Lambda_{1.4}$	727.071	639.032	686.786	730.737	790.051	390.005	301.388	274.908

4. SUMMARIES AND PERSPECTIVES

The latest density-dependent relativistic mean-field (DDRMF) parameterizations were systematically applied to investigate the properties of neutron star, i. e., DD2, DD-ME1, DD-ME2, DD-MEX, DD-LZ1, DDV, DDVT, and DDVTD sets. All of them were determined by fitting properties of spherical finite nuclei and have the same density-dependent function forms for meson coupling constants. Their densities, binding energies, incompressibilities, and symmetry energies at saturation points of symmetric nuclear matter are almost identical.

The equations of state (EOSs) of symmetric nuclear matter and pure neutron matter from present sets were separated into the softer type and stiffer one at high density region. The softer EOSs are generated by the DDV, DDVT, and DDVTD, whose coupling strengths of σ and ω mesons are weaker comparing to other sets. Their vector and scalar potentials have comparable magnitudes, while the vector potentials are much larger than the scalar ones in stiffer EOSs given by DD2, DD-ME1, DD-ME2, DD-MEX, and DD-LZ1. Their pressures in symmetric nuclear matter at $2 \sim 4\rho_{B0}$ were a little bit higher than the present constraints from heavy-ion collisions, while the softer EOSs satisfied these constraints.

The TOV equation was solved using the EOSs of neutron star matter, where the nucleons and leptons are in conditions of beta equilibrium and charge neutrality, generated by present DDRMF models. The softer EOSs from DDV, DDVT, and DDVTD only can support the neutron stars with maximum masses around $1.90 M_{\odot}$ at 10 km and tidal deformabilities at $1.4 M_{\odot}$, $\Lambda_{1.4} = 274 - 390$. The stiffer EOSs can generate very massive neutron stars around $2.5 M_{\odot}$. In particular, the DD-MEX and DD-LZ1 parameter sets even can produce neutron stars with masses of $2.55 M_{\odot}$, which can explain the secondary object in GW190814 with a mass of $2.50 - 2.67 M_{\odot}$. Furthermore, their radii at $1.4 M_{\odot}$ are also consistent with the constraints from NICER including the mass and radius simultaneous measurement, although their $\Lambda_{1.4}$ were around $639 - 790$.

In this investigation, we found that several parameterizations in DDRMF can provide very massive neutron stars due to the strong repulsive contributions from vector mesons at high density, which can describe ground state properties of finite nuclei exactly at the same time. The stiffer EOSs may slightly exceed the constraints of EOS from heavy-ion collisions and tidal deformability from GW170817. However, due to the strong model dependence of these two constraints and their large uncertainties, we can not exclude the possibility of the secondary object of GW190814 as a neutron star consisting of nucleons and leptons. We have shown that the stiffer EOSs give the dimensionless tidal

deformability around 100 for $2 M_{\odot}$ massive neutron star, while the softer ones less than 10. Therefore, the more precise measurement of dimensionless tidal deformability by the gravitational wave detectors will help us to determine the proper EOSs in the future. The density dependence of coupling constant in DDRMF model provides a good mechanism, which can describe probably the finite nuclei and supranuclear matter concurrently.

5. ACKNOWLEDGMENTS

This work was supported in part by the National Natural Science Foundation of China (Grants No. 11775119, No. 11675083, and No. 11405116), the Natural Science Foundation of Tianjin, and China Scholarship Council (Grant No. 201906205013 and No. 201906255002).

REFERENCES

- Abbott, B. P., Abbott, R., Abbott, T. D., et al. 2017a, *PhRvL*, 119, 161101
- Abbott, B. P., Abbott, R., Abbott, T. D., et al. 2017b, *ApJL*, 848, L12
- Abbott, B. P., Abbott, R., Abbott, T. D., et al. 2018, *PhRvL*, 121, 161101
- Abbott, B. P., Abbott, R., Abbott, T. D., et al. 2019, *PhRvX*, 9, 011001
- Abbott, B. P., Abbott, R., Abbott, T. D., et al. 2020a, *ApJL*, 892, L3
- Abbott, B. P., Abbott, R., Abbott, T. D., et al. 2020b, *ApJL*, 896, L44
- Akmal, A., Pandharipande, V. R., & Ravenhall, D. G. 1998, *PhRvC*, 58, 1804
- Annala, E., Gorda, T., Kurkela, A., & Vuorinen, A. 2018, *PhRvL120*, 172703
- Antoniadis, J., Freire P. C., Wex N., et al. 2013, *Sci*, 340, 6131
- Bao, S., Hu, J., Zhang, Z., & Shen, H. 2014a, *PhRvC*, 90, 045802
- Bao, S., & Shen, H. 2014b, *PhRvC*, 89, 045807
- Boguta, J. & Bodmer, A.R. 1977, *NuPhA*, 292, 414
- Bouyssy, A., Mathiot, J. F., Van Giai, N., & Marcos S. 1987 *PhRvC*, 36, 380
- Brockmann, R. 1978, *PhRvC*, 18, 1510
- Brockmann, R., & Toki, H. 1992, *PhRvL*, 68, 3408
- Carlson, J., Gandolfi, S., Pederiva, F., et al. 2015, *RvMP*, 87, 1067
- Cromartie, H. T., Fonseca, E., Ransom, S. M., et al. 2020, *NatAs*, 4, 72
- Danielewicz, P., Lacey, R., & Lynch, W. G. 2002, *Sci*, 289, 1592
- Demorest, P., Pennucci, T., Ransom, S., & Roberts, M. S. E. 2010, *Natur*, 467, 1081
- Douchin, F., & Haensel, P. 2001, *A&A*, 380, 151
- Dutra, M., Lourenco, O., Martins, J. S. Sá, et al. 2012, *PhRvC*, 85, 035201
- Dutra, M., Lourenco, O., Avancini, S. S., et al. 2014, *PhRvC*, 90, 055203
- Fattoyev, F. J., Horowitz, C. J., Piekarewicz, J. & Reed B. 2020, arXiv: 2007.03799
- Fonseca, E., Pennucci, T. T, & Ellis, J. A., et al. 2016, *ApJ*, 832, 167
- Hinderer, T. 2008, *ApJ*, 677, 1216
- Hinderer, T., Lackey, B. D., & Lang, R. N. 2010, *PhRvD*, 81, 123016
- Horowitz, C. J., & Piekarewicz, J. 2001, *PhRvL*, 86, 5647
- Hu, J., Zhang, Y., Epelbaum, E., Meißner, U. -G., & Meng, J. 2017, *PhRvC*, 96, 034307
- Hu, J., Bao, S., Zhang, Y., Nakazato, K., Sumiyoshi, K. & Shen, H. 2020, *PTEP*, 2020, 043D01
- Ji, F., Hu, J., Bao, S., & Shen, H. 2019, *PhRvC*, 100, 045801
- Lalazissis, G. A., Köning, J & Ring P. 1997, *PhRvC*, 55, 540
- Lalazissis, G. A., Nikšić, T., Vretenar, D. & Ring, P. 2005, *PhRvC*, 71, 024312
- Li, Z., Lombardo, U., Schulze, H. -J., et al. 2006, *PhRvC*, 74, 047304
- Lim, Y., Bhattacharya, A., Holt, J. W., & Pati, D. 2020, arXiv: 2007.06526
- Logoteta, D. 2019, *PhRvC*, 100, 045803
- Long, W. H., Meng, J., Van Giai, N., & Zhou, S. G., 2004 *PhRvC*, 69, 034319
- Long, W. H., Van Giai, N., & Meng, J. 2006, *PhLB*, 640, 150
- Long, W. H., Sagawa, H., Van Giai, N., & Meng, J. 2007, *PhRvC*, 76, 034314
- Miller, M. C., Lamb, F. K., Dittmann, A. J., et al. 2019, *ApJL*, 887, L24
- Nikolaus, B. A., Hoch, T., & Madland D. G., 1992, *PhRvC*, 46, 1757
- Nikšić, T., Vretenar, D., Finelli, P., & Ring, P. 2002, *PhRvC*, 66, 024306
- Oppenheimer, J. R. & Volkoff, G. M. 1939, *PhRe*, 55, 374
- Raaijmakers, G., Riley, T. E., Watts, A. L., et al. 2019, *ApJL*, 887, L22
- Riley, T. E., Watts, A. L., Bogdanov, S., et al. 2019, *ApJL*, 887, L21
- Sugahara, Y. & Toki, H. 1994, *NuPhA*, 579, 557
- Sammarruca, F., Marcucci, L. E., Coraggio, L., et al. 2018, arXiv:1807.06640
- Serot B. D. 1979, *PhLB*, 86, 146
- Shen, H. 2002, *PhRvC*, 65, 035802
- Shen, H., Toki, H., Oyamatsu, K., Sumiyoshi, K. 1998, *NuPhA*, 637, 435
- Sun, B., Long, W., Meng, J., & Lombardo, U. 2008, *PhRvC*, 78, 065805
- Tan, H., Noronh-Hostler, J., & Yunes, N. 2020, arXiv: 2006.16296
- Taninah, A., Agbemava, S.E., Afanasjev, A.V., Ring, P. 2020, *PhLB* 800, 135065
- Tews, I., Pang, P. T. H., Dietrich, T. & Coughlin, M. W. 2020, arXiv: 2007.06057
- Tolman, R. C. 1939, *PhRe*, 55, 364
- Toskaros, A., Ruiz, M., & Shapiro, S. L. 2020, arXiv: 2007.05526
- Typel, S., Röpke, G., Klähn, T., Blaschke, D., & Wolter, H. H. 2010, *PhRvC*81, 015803
- Typel S., & Terrero, D. A. 2020, *EPJA*, 56,160
- Vautherin D., & Brink, D. M. 1972, *PhRvC*, 5, 626
- Walecka, J. D. 1974, *AnnPh.*, 83, 491
- Wang, C., Hu, J., Zhang, Y., & Shen, H. 2020, *ApJ*, 897, 96
- Wei, B., Zhao, Q., Wang, Z. H., et al. 2020, *ChPhC*, 44, 074107
- Zhang, N. B., & Li, B. A. 2020, arXiv: 2007.02513
- Zhang, Y., Liu, M., Xia, C., Li, Z., & Biswal, S. K. 2020, *PhRvC*, 101, 034303
- Zhao, P. W., Li, Z. P., Yao, J. M., & Meng J. 2010, *PhRvC*, 82, 054319